Rev.Adv.Mater.Sci. 15(2007) 198-207

STRUCTURE AND MAGNETIC PROPERTIES OF C/FePt GRANULAR MULTILAYERS PREPARED BY ION-BEAM SPUTTERING

D. Babonneau[1], F. Pailloux[1], G. Abadias[1], F. Petroff[2], N.P. Barradas[3] and E. Alves[3]

[1]Laboratoire de Métallurgie Physique, UMR 6630 CNRS, Université de Poitiers, SP2MI, Téléport 2, Boulevard M. & P. Curie, BP 30179, 86962 Futuroscope Chasseneuil Cedex, France
[2]Unité Mixte de Physique CNRS/Thales associée à l'Université Paris-Sud XI, Route départementale 128, 91767 Palaiseau Cedex, France
[3]Instituto Technológico e Nuclear, E.N. 10, Apartado 21, 2686-953 Sacavém, and Centro de Física Nuclear da Universidade de Lisboa, Av. Prof. Gama Pinto 2, 1649-003 Lisboa, Portugal

Received: January 22. 2007

Abstract. Ion-beam sputtering has been used to achieve the growth of FePt thin films and C/FePt granular multilayers at room temperature. The effects of thermal annealing on the structural and magnetic properties have been investigated by transmission electron microscopy, Rutherford back-scattering spectrometry, grazing incidence X-ray diffraction, grazing incidence small-angle X-ray scattering, and magnetization measurements. The as-deposited films and granular multilayers show FePt grains (10-20 nm and 2-3 nm in size, respectively) with a disordered face-centered-cubic structure and are magnetically soft. Thermal annealing at temperatures below 650 °C causes partial $L1_0$ ordering and growth of the FePt grains to 100-200 nm in the FePt films and to 5-8 nm in the C/FePt multilayers. Thermal annealing of the granular multilayers at 800 °C also results in the preferential graphitization of the carbon matrix and chemical interaction of the Fe atoms with the Si substrate. Magnetization measurements indicate that magnetic hardening occurs after annealing and that the saturation magnetization of the granular multilayers is strongly dependent on the annealing temperature.

1. INTRODUCTION

Nanoscale magnetic systems are attracting considerable attention due to their potential in the field of ultrahigh density magnetic recording media [1]. To achieve high storage densities beyond 1 Tbit/in^2, assemblies of ferromagnetic monodomain are required. However, as the magnetic bit size is further reduced to the superparamagnetic limit, the magnetization of the particles is easily perturbed by thermal agitation. In order to overcome superparamagnetism, recent studies have been focused on CoPt and FePt nanoparticle arrays owing mainly to the existence of chemically ordered phases with exceptional magnetic properties such as large magnetocrystalline anisotropy constant above 10^7 erg/cm^3 [2,3]. Additional requirements for future magnetic recording media is that the nanoparticles have to be magnetically isolated but also chemically and mechanically stable. Therefore, much research work has been done on granular thin films

Corresponding author: D. Babonneau, e-mail:david.babonneau@univ-poitiers.fr

consisting of CoPt and FePt nanoparticles embedded in various nonmagnetic matrices (SiO_2 [4-6], Si_3N_4 [7], Al-O [8,9], B_2O_3 [10,11], BN [12,13], and C [13-19]). Among the prospective materials, C/CoPt and C/FePt granular thin films have attracted great interest because carbon not only hinders the growth of the nanoparticles, but also provides protection against outside degradations and reduces interparticle exchange interactions [20,21].

In general, CoPt and FePt nanoparticles in carbon-based granular films fabricated by sputtering processes at low substrate temperature have a disordered face-centered-cubic (fcc) structure (*A*1 phase), which is magnetically soft. In order to transform the as-deposited nanoparticles into the ordered face-centered-tetragonal (fct) structure ($L1_0$ phase), post-annealing at temperatures above 500 °C is necessary. Hence, it is predicted that the control of the magnetic properties of these granular thin films should be possible by adjusting the film composition, annealing temperature, and time. However, concurrently with chemical ordering, thermal treatment also causes particle growth and coalescence, which may adversely affect the magnetic properties. The study of the mechanisms responsible for the structural changes during the annealing process is therefore one of the key issues for future applications.

In the present article we focus on FePt films and C/FePt granular multilayers grown by ion-beam sputtering and post-annealed in vacuum. Structural and magnetic properties of the as-deposited and post-annealed multilayers are investigated by combining the sensibilities of different techniques including transmission electron microscopy in conventional (CTEM), high-resolution (HRTEM) and energy-filtered (EFTEM) modes, Rutherford backscattering spectrometry (RBS), grazing incidence X-ray diffraction (GIXRD), grazing incidence small-angle X-ray scattering (GISAXS), and superconducting quantum interference device (SQUID) magnetometry.

2. EXPERIMENTAL DETAILS

FePt (*t* nm) films (with thickness *t*=41 and 50 nm) and C (4.3 nm)/[FePt (1.1 nm)/C (4.3 nm)]$_N$ multilayers (with number of FePt/C bilayers *N*=1, 20, and 40) were fabricated at room temperature by ion-beam sputtering of high purity C and FePt targets. The base pressure in the deposition chamber was $2{\cdot}10^{-8}$ Torr and the sputtering process was carried out at $2{\cdot}10^{-4}$ Torr by using an Ar^+ ion-beam operated at 1.2 keV and 80 mA.

The FePt (41 nm) film was deposited on freshly cleaved NaCl substrates, which were floated in purified water. The resulting free-standing films were finally collected on molybdenum grids for *in situ* characterization during thermal annealing by CTEM using a JEOL 200CX microscope operated at 200 keV. The other samples deposited on surface oxidized Si(001) substrates were post-annealed in vacuum at different temperatures ranging from 500 to 800 °C and were analyzed by various *ex situ* techniques. The FePt (50 nm) film and C/[FePt/C]$_{40}$ multilayers were characterized by GIXRD carried out at the European Synchrotron Radiation Facility (ESRF, Grenoble) on beamline BM32. The samples were kept vertical during the course of the measurements and the incident wavelength was fixed to 0.11 nm. The angle of incidence was ω=1° and the diffracted intensities were measured with the scattering angle being varied from 2θ=10° to 62°. This geometry confines the scattering vector perpendicular to the growth direction, which gives information on the in-plane lattice parameter.

The C/[FePt/C]$_1$ and C/[FePt/C]$_{20}$ multilayers were analyzed by RBS to determine the stoichiometry of the FePt layers and the average C/FePt bilayer density. A 2.0 MeV He^+ beam with 15 keV energy resolution detected at 160° in the Cornell geometry was used. The angle of incidence φ, defined as the angle between the beam and the normal to the sample, was varied between 70° and 82°. Morphology and spatial organization of the FePt nanoparticles were studied by GISAXS performed at the LURE synchrotron source on beamline DW31B. The energy of the incident photons was 7 keV and the angle of incidence with respect to the surface was ω=0.3°. The transmitted and specularly reflected beams were masked by a vertical beam-stop and the scattering was monitored in the (q_y,q_z) reciprocal space with a charge-coupled device 2D detector located 380 mm away from the sample. The microstructure of the as-deposited and post-annealed C/[FePt/C]$_{20}$ multilayers was examined by cross-sectional HRTEM performed with a JEOL 3010 microscope equipped with a LaB_6 emitter and operated at 300 keV. The multilayer annealed at 800 °C was examined by EFTEM using a JEOL 2200FS microscope equipped with an in-column omega filter and a field emission gun operated at 200 keV. The 3-window technique was employed and the chemical maps for Fe, Si, and C were respectively acquired at the energies of the Fe-$L_{2,3}$ (710 eV), Si-

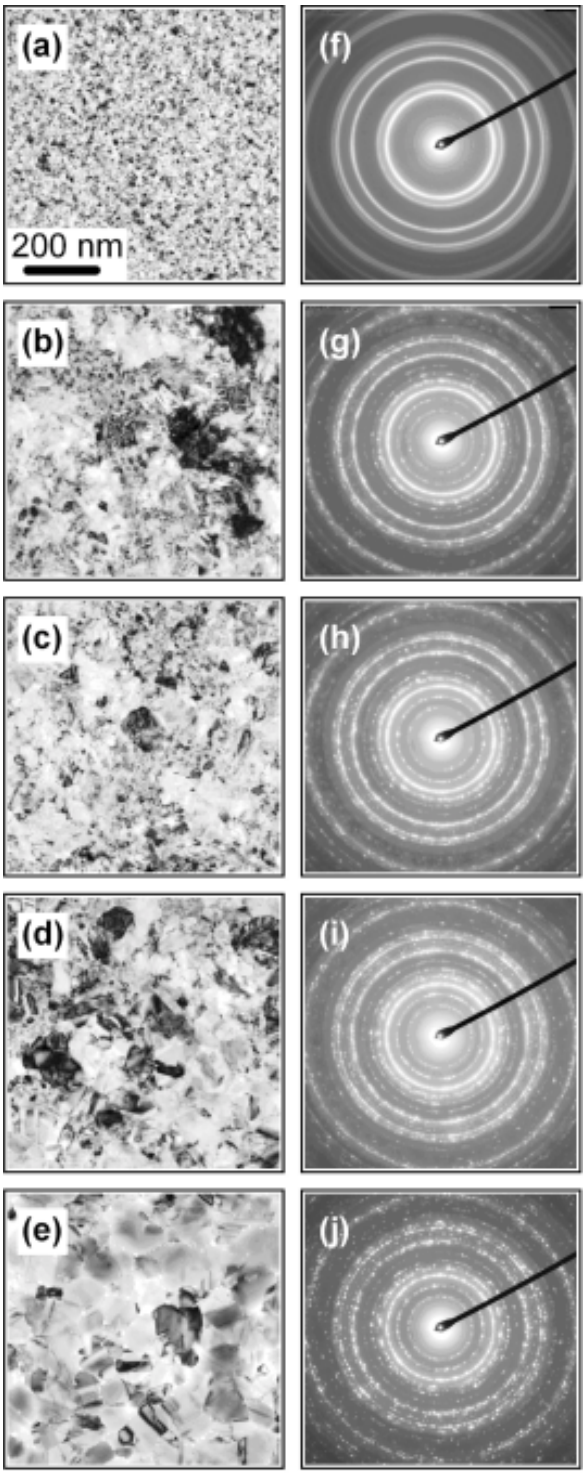

Fig. 1. Plane-view CTEM micrographs and corresponding SAED patterns obtained during *in situ* thermal annealing of the FePt (41 nm) film: (a,f) as-deposited, (b,g) 350 °C, (c,h) 450 °C, (d,i) 550 °C, and (e,j) 650 °C.

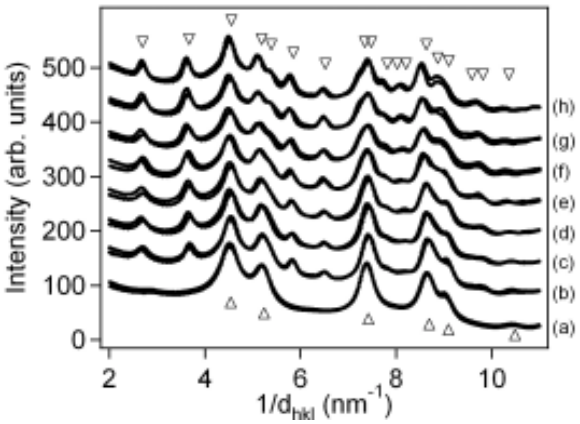

Fig. 2. Electron diffraction profiles of the FePt (41 nm) film obtained from the SAED patterns collected during *in situ* thermal annealing: (a) as-deposited, (b) 350 °C, (c) 400 °C, 450 °C (d), 500 °C (e), 550 °C (f), 600 °C (g), and 650 °C (h). The position of the lines expected for the disordered *A*1 (up triangles) and ordered $L1_0$ (down triangles) FePt phases is also indicated.

$L_{2,3}$ (99 eV) and C-K (285 eV) edges. The energy width of the selecting slit was set to 30 eV.

Magnetic properties were measured at 150K using a Quantum Design SQUID magnetometer with a magnetic field between ±50 kOe applied parallel to the plane of the films.

3. RESULTS AND DISCUSSION

3.1. Chemical ordering of FePt films and C/[C/FePt]$_{40}$ multilayers

Figs. 1a–1j show representative plane-view CTEM micrographs and corresponding selected area electron diffraction (SAED) patterns obtained during *in situ* thermal annealing of the FePt (41 nm) film. The electron diffraction profiles extracted from the SAED patterns are displayed in Fig. 2 together with the position of the main lines for the disordered *A*1 and ordered $L1_0$ FePt phases [22]. As expected, the as-deposited film is polycrystalline and consists of randomly oriented fcc FePt grains with size in the range 10-20 nm. Post-annealing not only causes grain growth (size in the range 100-200 nm at 650 °C), but also undergoes a progressive phase transformation from the disordered fcc to the ordered fct structure. This is characterized by the appearance of additional rings in the SAED pat-

terns of the annealed films that are not present in the as-deposited film.

In agreement with the CTEM results, the GIXRD pattern of the as-deposited FePt (50 nm) film [Fig. 3a] shows reflections corresponding to a fcc structure with a lattice parameter a=3.825 Å close to the lattice constant of the disordered $A1$ FePt phase a_{bulk}=3.816 Å [22]. In comparison, due to the presence of very small FePt grains, broader peaks are observed in the GIXRD pattern of the as-deposited C[C/FePt]$_{40}$ multilayer [Fig. 3b] with the main (111) peak yielding a=3.79 Å. This lattice contraction of ~1% may be attributed to small-size effects [23] or to the presence of compressive stress currently observed in ion-beam sputtered films [24,25]. In addition, two bumps located around $2\theta\approx18°$ and around $2\theta\approx52°$ are observed in the GIXRD pattern of the as-deposited C[C/FePt]$_{40}$ multilayer. The latter can be interpreted as the merging of the (220), (311) and (222) peaks into one because of an amorphous-like structure of the FePt grains. The former might be due to the presence of nanometric graphite-like domains in the carbon matrix or to the presence of poorly crystallized tetragonal FePt grains. After annealing at 600 °C for 1 h, the GIXRD pattern of the C[C/FePt]$_{40}$ multilayer [Fig. 3c] clearly evidences the formation of the ordered $L1_0$ FePt phase, which is characterized by the appearance of the (001) and (110) superlattice peaks. However, the splitting of the (200)-(002) reflections is not observed because of their close position and the broadening of these peaks. The lattice parameters of the ordered FePt phase were deduced from the positions of the (100) and (110) Bragg reflections. The obtained values, $a\approx3.94$ Å and $c\approx3.61$ Å, attest a strong tetragonality ($c/a\approx0.92$) as compared to the bulk $L1_0$ phase (a_{bulk}=3.853 Å, c_{bulk}=3.713 Å, c/a=0.96 [22]). The long-range order parameter, S, was estimated from the ratio of the integrated intensities of the (001) and (110) superstructure peaks versus the (002) and (220) fundamental peaks, following the analysis described in Refs. 26 and 27. This parameter may vary between S=0 for a fully disordered FePt alloy to S=1 for the perfectly ordered alloy. In the present case, we assumed the same Debye-Waller parameter B for both Pt and Fe atoms and a homogeneous ordering within all FePt grains (i.e., the volume fraction of the film which is chemically ordered is equal to 1.0). This yields S=0.55, indicating that partial ordering takes place at 600 °C. This result is consistent with the value reported in the literature for 5 nm-FePt nanoparticles embedded in carbon [16].

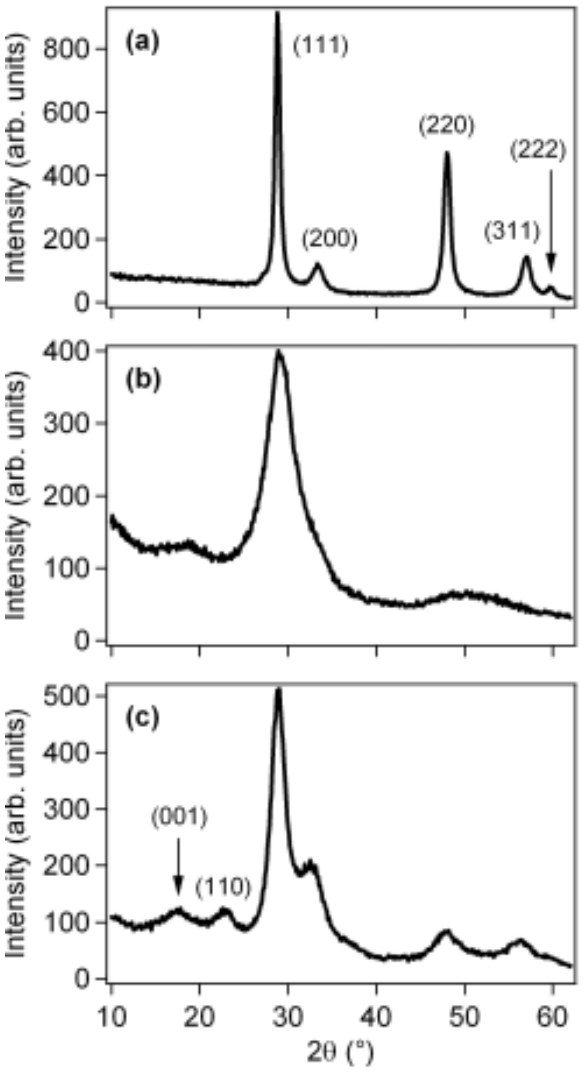

Fig. 3. GIXRD patterns of the (a) as-deposited FePt (50 nm) film, (b) as-deposited C/[C/FePt]$_{40}$ multilayer, and (c) C/[C/FePt]$_{40}$ multilayer post-annealed at 600 °C for 1 h.

It is here important to point out that the estimation of the long-range order parameter from the c/a ratio [13] would lead to S=2, which is physically impossible, showing the inappropriateness of this type of analysis.

3.2. Structure of C/[C/FePt]$_{20}$ multilayers

The stoichiometry of the FePt layers was determined from RBS analysis of the C/[FePt/C]$_1$ multilayer. Within the experimental error, a 1:1 ratio was found [28]. Furthermore, 3 at.% Ar was found in

Table 1. Results obtained from the analysis of the RBS data collected for as-deposited and post-annealed C[(C/FePt]$_{20}$ multilayers for 1 h. The table includes the FePt areal density ([*FePt*]), the C areal density ([*C*]), and the average multilayer density (ρ) calculated using the bilayer thickness determined by GISAXS.

Sample	[*FePt*]/10^{15} (at/cm^2)	[*C*]/10^{15} (at/cm^2)	ρ/10^{23} (at/cm^3)
As-deposited	164 ± 10	1110 ± 50	1.16 ± 0.05
Annealed at 600 °C	154 ± 10	1050 ± 50	0.96 ± 0.05
Annealed at 800 °C	174 ± 10	1040 ± 50	0.94 ± 0.05

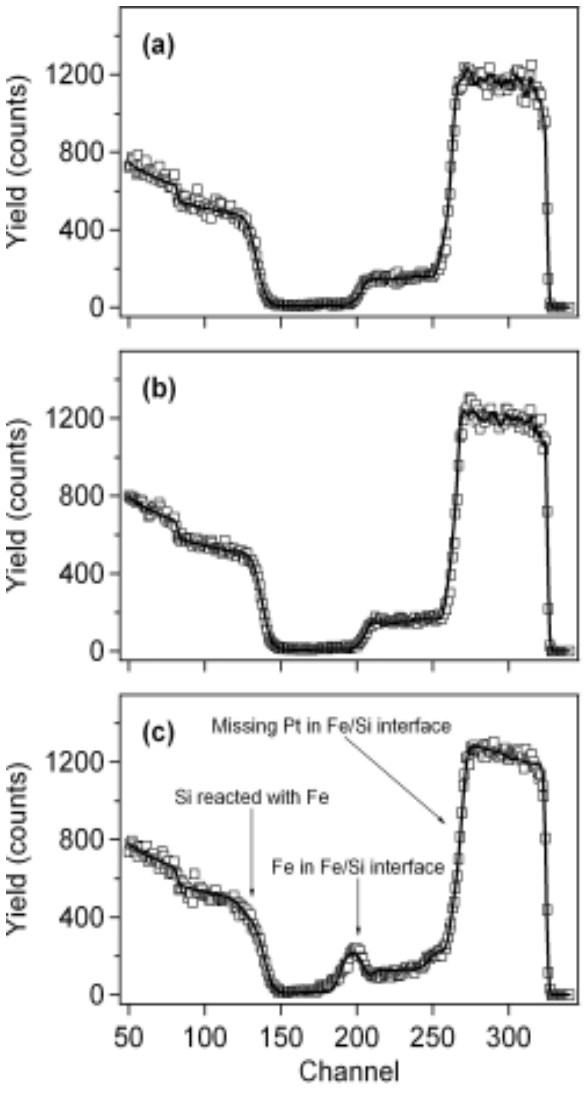

Fig. 4. RBS data (squares) collected at φ=75° for C/[C/FePt]$_{20}$ multilayers: (a) as-deposited, (b) post-annealed at 600 °C for 1 h, and (c) post-annealed at 800 °C for 1 h. The solid lines are the best fits to the experimental data.

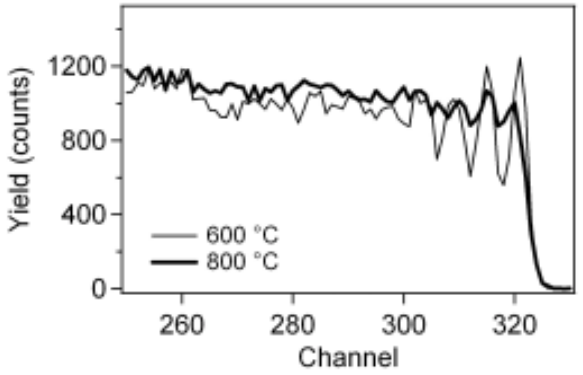

Fig. 5. RBS data collected at φ=82° for the C/[C/FePt]$_{20}$ multilayers post-annealed at 600 °C and at 800 °C for 1 h.

the FePt, and 0.4 at.% Mo was found in the C. Both are contamination due to the deposition system that includes Ar^+ sputtering ions and Mo extraction grids. These values were used in the analysis of the C/[FePt/C]$_{20}$ multilayers. Figs. 4a–4c shows the RBS data collected at φ=75° from as-deposited and post-annealed C/[FePt/C]$_{20}$ multilayers. These data were analyzed with the IBA DataFurnace [29] to determine the total amounts of FePt and C atoms in the multilayers. The results reported in Table 1 clearly show that the total amounts of FePt and C atoms remain constant even after thermal annealing at 800 °C for 1 h. However, it is evident that annealing at 800 °C causes chemical interaction of FePt layers with the Si substrate as was already observed in FePt-Si_3N_4 cosputtered films [7]. Actually, one can argue that Fe atoms are diffused into the substrate and reacted with Si atoms, as we observe an enhanced Fe signal at the substrate/film interface accompanied by a lack of Pt counts. It should be also noted that within the depth reso-

Table 2. Results obtained from the analysis of the GISAXS data collected for as-deposited and post-annealed C[(C/FePt]$_{20}$ multilayers. The table includes the bilayer thickness (Λ_z), the average diameter (<*D*>), and the in-plane interparticle distance (Λ_y).

Sample	Λ_z (nm)	<*D*> (nm)	Λ_y (nm)
As-deposited	5.49	2.52	5.22
Annealed at 500 °C for 2 h	6.10	4.02	5.63
Annealed at 600 °C for 1 h	6.26	5.05	6.85
Annealed at 700 °C for 1 h	6.47	8.04	∞
Annealed at 800 °C for 1 h	6.43	9.03	∞

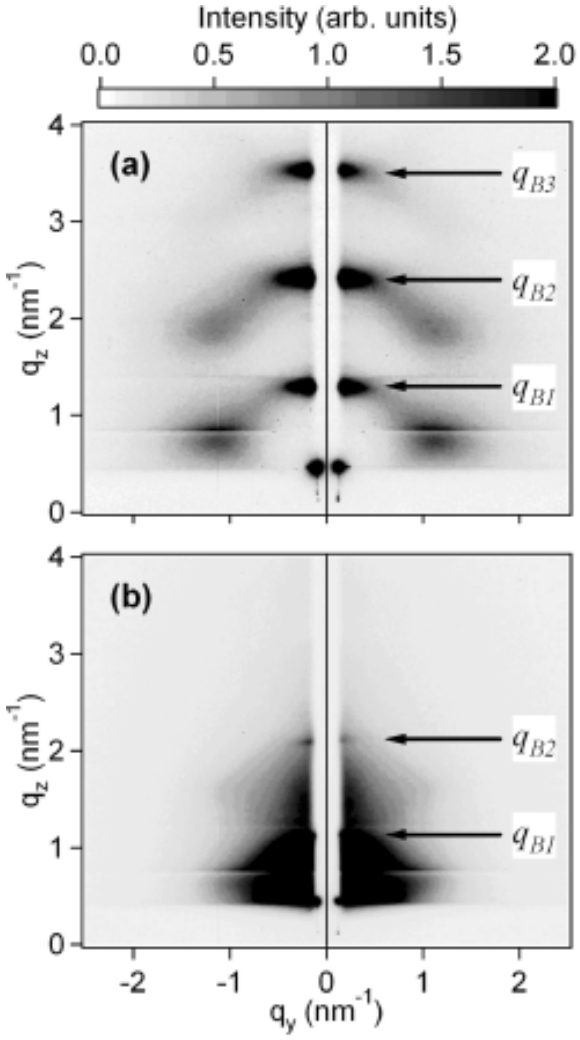

Fig. 6. 2D GISAXS patterns of the C/[C/FePt]$_{20}$ multilayers: (a) as-deposited and (b) post-annealed at 600 °C for 1 h.

lution of the experiment, this only affects the layers closer to the Si substrate, while the layers closer to the surface do not react with the Si atoms. In addition, experiments made at more grazing angles reveal a strong multilayer signal for the samples as-deposited (not shown) and post-annealed at 600 °C for 1h (Fig. 5), which proves a well-defined vertical ordering. As seen in Fig. 5, a much smaller multilayer signal is observed after annealing at 800 °C for 1 h, indicating a much less regular ordering.

2D GISAXS patterns of C/[C/FePt]$_{20}$ multilayers collected from a large sample area of about 15 mm^2 are compared in Fig. 6. In the pattern of the as-deposited sample [Fig. 6a], it is immediately apparent that there is an intense nonspecular diffuse scattering at low q_y giving rise to three transverse Bragg peaks. Their presence at well-defined q_z-positions (labelled q_{B1}, q_{B2}, and q_{B3}) is typical of a highly periodic system with period Λ_z=5.49 nm in agreement with the nominal bilayer thickness (5.4 nm). Conversely, transverse Bragg peaks in the 2D GISAXS pattern of the multilayer annealed at 600 °C for 1 h [Fig. 6b] are less intense, which is characteristic of a less ordered system. The Λ_z values determined for all the as-deposited and post-annealed C/[C/FePt]$_{20}$ multilayers are gathered in Table 2. Furthermore, we reported in Table 1 the average multilayer density estimated from the following relation: $\rho=([FePt]+[C])/(N\Lambda_z)$, where [*FePt*] and [*C*] are the FePt and C areal densities determined from RBS analysis. It is clear that the average bilayer thickness increases with the annealing temperature whereas the average multilayer density decreases. This is most likely due to the partial graphitization of the carbon matrix under thermal annealing as already observed in other metal/carbon systems [30,31]. Another distinctive feature noticed in the 2D GISAXS pattern of the as-deposited multilayer is a coherent small-angle scattering from isolated nanoparticles giving rise to six diffuse spots centered around q_y=±1.10 nm^{-1} and $q_z \approx q_{B1}/2$ (first order), $q_z \approx (q_{B1}+q_{B2})/2$ (second order),

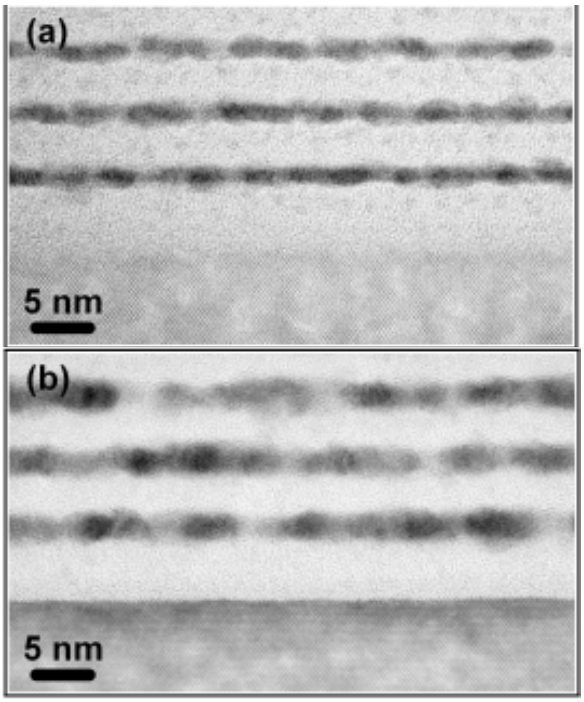

Fig. 7. HRTEM cross-section micrographs of the C/[C/FePt]$_{20}$ multilayers: (a) as-deposited and (b) post-annealed at 600 °C for 1 h.

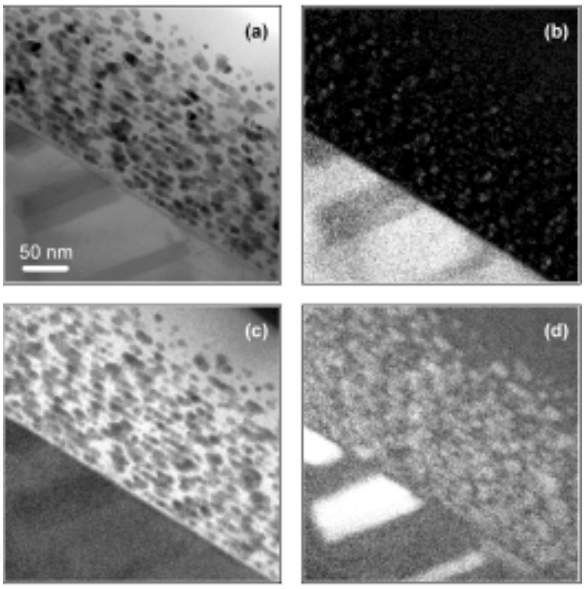

Fig. 8. EFTEM image series of the C/[C/FePt]$_{20}$ multilayer post-annealed at 800 °C for 1 h. (a) Zero-loss bright field image, (b) silicon map, (c) carbon map, (d) iron map.

and $q_z \approx (q_{B2}+q_{B3})/2$ (third order). This suggests that the vertical arrangement of the FePt nanoparticles from layer to layer is not random in the as-deposited multilayer, but shows a topology-induced self-organization [32]. In the 2D GISAXS pattern of the multilayer annealed at 600 °C for 1 h, the diffuse spots concentrates towards the origin of the reciprocal space, which is typical of particles coarsening. The results obtained from the quantitative analysis of the GISAXS data using the monodisperse approximation [32] are reported in Table 2, i.e. the average particle diameter (<*D*>) and the in-plane interparticle distance (Λ_y). These results illustrate the progressive transformation of the granular multilayer from a system of small correlated nanoparticles at low temperatures (≤600 °C) to a system of large uncorrelated nanoparticles ($\Lambda_y=\infty$) at high temperatures (≥700 °C). Therefore, we can suggest that the coarsening of the post-annealed particles results first from thermally activated migration of Fe and Pt atoms at low temperatures and then from coalescence phenomena at high temperatures. However, in comparison with pure FePt films (Fig. 1), it is clear that carbon restrains grain growth during thermal annealing.

Fig. 7 shows the microstructure typical of C[C/FePt]$_{20}$ multilayers as observed by HRTEM cross-sections. The micrograph of the as-deposited specimen [Fig. 7a] clearly exhibits a layered structure, which appears as planes of dark FePt nanograins separated by amorphous carbon layers. The FePt nanograins have the shape of oblate spheroids with lateral diameter around 3 nm in agreement with the GISAXS results and aspect ratio (height/diameter) of about 2/3. After annealing at 600 °C for 1 h [Fig. 7b], the size of the FePt nanograins has increased both in lateral and vertical dimensions and the matrix appears as graphite-like carbon, which confirms also the GISAXS results. Moreover, it is worth noting that the HRTEM micrographs of both the as-deposited and post-annealed specimens reveal that the C and FePt layers do not react with the Si(001) substrate. In contrast, the chemical interaction of the Fe atoms with the Si substrate after annealing at 800 °C is directly evidenced in the EFTEM images displayed in Fig. 8. The zero-loss bright field image [Fig. 8a] not only confirms that the vertical periodicity of the multilayer tends to be destroyed, but also shows that precipitates oriented at 54° with respect to the

Table 3. Magnetic properties of as-deposited and post-annealed C[(C/FePt]$_{20}$ multilayers determined from hysteresis loops measured at 150K. The table includes the coercivity (H_c), the saturation magnetization (M_s), and the remanence ratio (M_r/M_s).

Sample	H_c (Oe)	M_s (emu/cm^3)	M_r/M_s
As-deposited	14	730	0.61
Annealed at 500 °C for 2 h	132	1050	0.12
Annealed at 800 °C for 1 h	1842	590	0.42

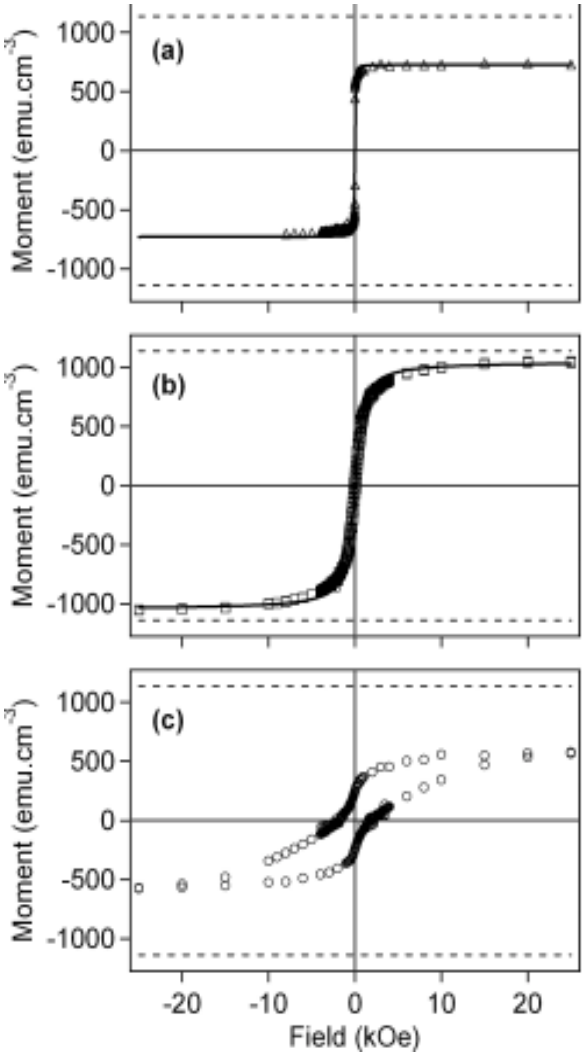

Fig. 9. Hysteresis loop of the C/[C/FePt]$_{20}$ multilayers: (a) as-deposited, (b) post-annealed at 500 °C for 2 h, and (c) post-annealed at 800 °C for 1 h. The solid lines are the best Langevin fits to the experimental data. The dotted lines represent the M_s value expected for fully ordered $L1_0$ FePt nanoparticles.

Si/C interface (<111> directions) are formed in the Si substrate. In addition, the chemical maps [Figs. 8b–8d] show the presence of Fe both in the FePt grains of the multilayer and in the oriented precipitates of the substrate, while the Si signal is decreased in the oriented precipitates. Moreover, the carbon map proves that diffusion of carbon across the interface with the Si substrate has not occurred (a sharp edge of the C signal is observed at the inteface). Thus, this set of maps clearly evidences the crystallization of iron silicides precipitates coherent with the Si substrate.

3.3. Magnetic properties of C/[C/FePt]$_{20}$ multilayers

Hysteresis loops of C/[C/FePt]$_{20}$ multilayers measured at 150K are presented in Fig. 9. The corresponding coercivity, H_c, saturation magnetization, M_s, and remanence ratio, M_r/M_s, are listed in Table 3. The magnetization curves $M(H)$ of the multilayers as-deposited [Fig. 9a] and post-annealed at 500 °C for 2 h [Fig. 9b] show a soft magnetic feature with low coercivity, suggesting that the FePt nanoparticles are thermally unstable, i.e., they are in the superparamagnetic state. Under the assumption of weak interparticle interactions, the magnetization curve $M(H)$ of a superparamagnetic system can be described by a Langevin function:

$$M(H) = M_s\left[\coth(x) - \frac{1}{x}\right], \qquad (1)$$

where $x = M_s VH/k_B T$, k_B is the Boltzmann constant, and V is the particle volume. Assuming spherical magnetic particles with diameter D_m, the fits to the experimental data yield D_m=15.25 nm for the as-deposited multiliayer and D_m=4.49 nm for the multilayer post-annealed at 500 °C for 2 h. Whereas the magnetic size D_m of the post-annealed particles

is found to be in good agreement with the structural size <*D*> determined by GISAXS, a strong discrepancy is revealed for the as-deposited particles ($D_m \approx 6\langle D\rangle$). Moreover, one can notice in Table 3 that the as-deposited multilayer presents a remanence ratio much higher than that of the post-annealed multilayer. These results suggest that strong exchange interactions actually exist between as-deposited FePt nanoparticles due to their proximity. In addition, the M_s value of the as-deposited multilayer is 730 emu/cm^3, which is less than the value of 1030 emu/cm^3 expected for disordered fcc FePt [33]. This reduction may be due to the presence of a significant amount of Fe and Pt atoms dissolved in the matrix. A further reason might be attributed to the presence of carbon atoms in the FePt phase or to reduced moments for the atoms at the surface of the nanoparticles. After annealing at 500 °C for 2 h, the saturation magnetization rises to M_s=1050 emu/cm^3, which is approaching the bulk value of 1140 emu/cm^3 for $L1_0$ FePt. This result confirms that partial $L1_0$ ordering arises under thermal annealing.

Another signature of annealing-induced $L1_0$ ordering is that the multilayer post-annealed at 800 °C for 1 h [Fig. 9c] shows hard magnetic properties with high coercivity of H_c=1.84 kOe and remanence ratio M_r/M_s=0.42, which is approaching the predicted value of 0.5 for noninteracting single domain particles with easy axes randomly oriented [34]. However, in Fig. 9c, it can be seen that a shoulder is present in the magnetization curve. It might be related to the presence of a soft magnetic phase that is not exchange coupled to the hard phase. Furthermore, the M_s value of the multilayer annealed at 800 °C for 1 h is strongly decreased to 590 emu/cm^3, which is most likely due to the diffusion of Fe atoms of the FePt layers into the substrate, as revealed by RBS and EFTEM experiments.

4. CONCLUSIONS

In this paper, we have explored the thermal annealing effects on the structural and magnetic properties of FePt films and C/FePt granular multilayers prepared by ion-beam sputtering. Our results show that the as-deposited films and multilayers contain FePt grains with a disordered face-centered-cubic structure and are magnetically soft. Thermal annealing not only causes the growth of the FePt grains but also induces partial $L1_0$ ordering, which results in a hardening of the magnetic properties. Nevertheless, it is worth noting that the presence of carbon around the FePt grains restrains their growth as well as their chemical ordering. This leads to an increase of the temperature required to transform the soft fcc FePt phase to the hard fct FePt phase. Furthermore, thermal annealing generates preferential graphitization of the carbon matrix, which leads to a gradual increase of the bilayer thickness, and chemical interaction of the Fe atoms with the Si substrate at 800 °C. Therefore, new routes are explored to facilitate the phase transformation at low temperatures such as ion irradiation [35] or metal additive [36].

ACKNOWLEDGEMENTS

We thank P. Guérin for his help during the preparation of the FePt films and C/FePt multilayers. We are grateful to M.F. Denanot for the CTEM characterizations of the FePt films and the HRTEM observations of the C/FePt multilayers. We acknowledge the assistance of O. Lyon and J.S. Micha during the GISAXS and GIXRD experiments.

REFERENCES

[1] N. Weiss, T. Kren, M. Epple, S. Rusponi, G. Baudot, S. Rohart, A. Tajeda, V. Repain, S. Rousset, P. Ohresser, F. Scheurer, P. Bencok and H. Brune // *Phys. Rev. Lett.* **95** (2005) 157204.

[2] S.H. Liou, Y. Liu, S.S. Malhotra, M. Yu and D.J. Sellmyer // *J. Appl. Phys.* **79** (1996) 5060.

[3] S. Sun, C.B. Murray, D. Weller, L. Folks and A. Moser // *Science* **287** (2000) 1989.

[4] Kaitsu, A. Inomata, I. Okamoto and M. Shinohara // *IEEE Trans. Mag.* **34** (1998) 1591.

[5] K. Ichihara, A. Kikitsu, K. Yusu, F. Nakamura and H. Ogiwara // *IEEE Trans. Mag.* **34** (1998) 1603.

[6] C.P. Luo and D.J. Sellmyer // *Appl. Phys. Lett.* **75** (1999) 3162.

[7] C.M. Kuo and P.C. Kuo // *J. Appl. Phys.* **87** (419) 2000.

[8] M. Watanabe, T. Masumoto, D.H. Ping and K. Hono // *Appl. Phys. Lett.* **76** (2000) 3971.

[9] D.H. Ping, M. Ohnuma, K. Hono, M. Watanabe, T. Isawa and T. Masumoto // *J. Appl. Phys.* **90** (2001) 4708.

[10] C.P. Luo, S.H. Liou, L. Gao, Y. Liu and D.J. Sellmyer // *Appl. Phys. Lett.* **77** (2000) 2225.

[11] M.L. Yan, H. Zeng, N. Powers and D.J. Sellmyer // *J. Appl. Phys.* **91** (2002) 8471.
[12] M. Daniil, P.A. Farber, H. Okumura, G.C. Hadjipanayis and D. Weller // *J. Magn. Magn. Mater.* **246** (2002) 297.
[13] J.A. Christodoulides, P. Farber, M. Daniil, H. Okomura, G.C. Hadjipanayis, V. Skumryev, A. Simopoulos and D. Weller // *IEEE Trans. Magn.* **37** (2001) 1292.
[14] J.J. Delaunay, T. Hayashi, M. Tomita, S. Hirono and S. Umemura // *Appl. Phys. Lett.* **71** (1997) 3427.
[15] M. Yu, Y. Liu, A. Moser, D. Weller and D.J. Sellmyer // *Appl. Phys. Lett.* **75** (1999) 3992.
[16] J.A. Christodoulides, M.J. Bonder, Y. Huang, Y. Zhang, S. Stoyanov, G.C. Hadjipanayis, A. Simopoulos and D. Weller // *Phys. Rev. B* **68** (2003) 054428.
[17] Perumal, H.S. Ko and S.C. Shin // *Appl. Phys. Lett.* **83** (2003) 3326.
[18] Y. Xu, M.L. Yan, J. Zhou and D.J. Sellmyer // *J. Appl. Phys.* **97** (2005) 10J320.
[19] W.B. Mi, H. Liu, Z.Q. Li, P. Wu, E.Y. Jiang and H.L. Bai // *J. Appl. Phys.* **97** (2005) 124303.
[20] T. Hayashi, S. Hirono, M. Tomita and S. Umemura // *Nature (London)* **381** (1996) 772.
[21] D. Babonneau, J. Briatico, F. Petroff, T. Cabioc'h and A. Naudon // *J. Appl. Phys.* **87** (2000) 3432.
[22] *Joint Committee on Powder Diffraction Standards,* 2000*. JCPDS-ICDD Powder Diffraction Database*, *cards No.* **29-718** *(A1 FePt)* and *No.* **43-1359** *($L1_0$ FePt), Swarthmore, Pennsylvania, USA.*
[23] C.R. Henry // *Surf. Sci. Rep.* **31** (1998) 231.
[24] H. Windischmann // *Crit. Rev. Solid State Mater. Sci.* **17** (1992) 547.
[25] Debelle, G. Abadias, A. Michel and C. Jaouen // *Appl. Phys. Lett.* **84** (2004) 5034.
[26] Cebollada, R.F.C. Farrow and M.F. Toney, In: *Magnetic Nanostructures, ed. by H.S. Nalwa* (American Scientific Publishers, 2002)*.*
[27] B.E. Warren*, X-ray Diffraction (Dover, New-York,* 1990*).*
[28] N.P. Barradas, E. Alves and D. Babonneau // *Nucl. Instrum. Methods Phys. Res. B.* **219-220** (2004) 919.
[29] N.P. Barradas, C. Jeynes and R. Webb // *Appl. Phys. Lett.* **71** (1997) 291.
[30] R. Lamber, N. Jaeger and G. Shulz-Ekloff // *Surf. Sci.* **197** (1988) 402; *ibid*, **227** (1990) 15; *ibid*, **289** (1993) 247.
[31] T.J. Konno and R. Sinclair // *Acta Metall. Mater.* **42** (1994) 1231.
[32] D. Babonneau, F. Petroff, J.-L. Maurice, F. Fettar, A. Vaurès and A. Naudon // *Appl. Phys. Lett.* **76** (2000) 2892.
[33] T. Thomson, S.L. Lee, M.F. Toney, C.D. Dewhurst, F.Y. Ogrin, C.J. Oates and S. Sun // *Phys. Rev. B* **72** (2005) 064441.
[34] E.C. Stoner and E.P. Wohlfarth // *Philos. Trans. R. Soc. London, Ser. A* **240** (1948) 599.
[35] H. Bernas, J.P. Attané, K.H. Heinig, D. Halley, D. Ravelosona, A. Marty, P. Auric, C. Chapper and Y. Samson // *Phys. Rev. Lett.* **91** (2003) 077203.
[36] J.W. Harrell, D.E. Nikles, S.S. Kang, X.C. Sun, Z. Jia, S. Shi, J. Lawson, G.B. Thompson, C. Srivastava and N.V. Seetala // *Scripta Mater.* **53** (2005) 411.